^{3}He magnetic form factor

P. C. Dunn,* S. B. Kowalski, F. N. Rad,† C. P. Sargent, and W. E. Turchinetz
Bates Linear Accelerator Center, Department of Physics and Laboratory for Nuclear Science, Massachusetts Institute of Technology, Cambridge, Massachusetts 02139

R. Goloskie and D. P. Saylor
Department of Physics, Worcester Polytechnic Institute, Worcester, Massachusetts 01601
(Received 4 June 1982)

The ^{3}He magnetic form factor has been measured for momentum transfers between 0.7 and 11 fm^{-2} with improved precision over previous measurements. The charge form factor has been measured for momentum transfers less than 1 fm^{-2}. The charge radius was determined to be 1.935±0.03 fm, and the magnetic radius 1.935±0.04 fm. Comparisons are made with calculations which include meson exchange corrections and reasonable agreement is found.

[NUCLEAR REACTIONS $d(e,e')d$, $q^2=0.7$ to 11 fm^{-2}, $\theta=160°$, measured magnetic form factor; $q^2<1$ fm^{-2}, $\theta=60°$, measured charge radius.]

INTRODUCTION

Electron scattering cross sections of the three-body systems, ^{3}He and ^{3}H, are among the most important observables of nuclear physics. On one hand, given the local charge and current distributions of the scattering system, the cross section may be calculated reliably using quantum electrodynamics. On the other hand, modern methods for solving the nuclear three-body problem have been developed to a sufficient state so that discrepancies between a measured cross section and that calculated from the charge and current distributions yielded by the theory must arise from deficiencies in the basic theory rather than from inaccurate approximations in the calculation. In particular, the failure of the wave functions calculated using variational or Faddeev methods and a variety of phase-shift equivalent *NN* potentials to account for the charge form factor of ^{3}He has led to extensive investigations of meson exchange currents, three-body forces and/or isobar configurations in the ground state, relativistic corrections, and, at the highest momentum transfers, quark degrees of freedom. (See Ref. 1 for a recent review of this problem.)

While the data base for the elastic charge form factor extends over the range $0.03<q^2<100$ fm^{-2} and provides a good set of constraints on the further development of the theory, the available data[2,3] for the magnetic form factor are neither as extensive nor as accurate. Thus, the data covers only the range $1<q^2<16$ fm^{-2} and have quoted uncertainties of 20% or greater. These data are compared in Fig. 1 with two recently calculated form factors[4,5] which differ in various details but which include the effect of meson-exchange currents. In this

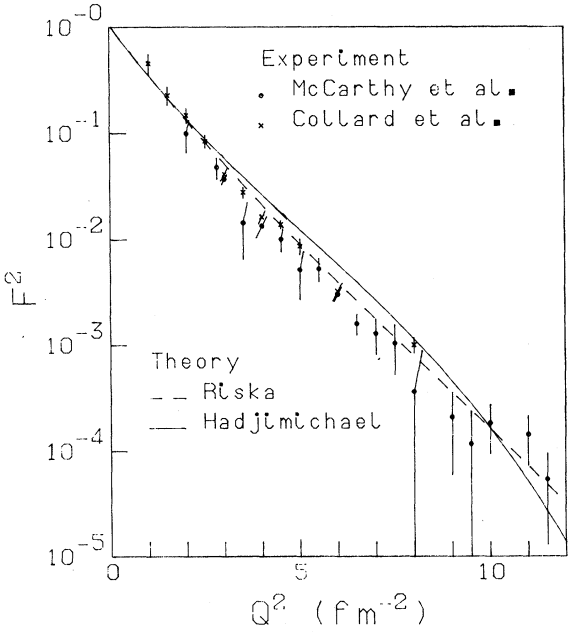

FIG. 1. Previous experimental determinations of the magnetic form factor of ^{3}He by Collard *et al.* (Ref. 2) and McCarthy *et al.* (Ref. 3). The theories are due to Borroso and Hadjimichael (Ref. 4) and Riska (Ref. 5). The results are displayed as a function of q^2.

range of momentum transfers, owing to a destructive interference between the S and D state matrix elements of the single nucleon current operator, there appears a minimum in the classical form factor between 6 and 8 fm^{-2}. Inclusion of meson-exchange currents remedies this defect, and indeed the cross section in this range of q^2 is dominated by two-body currents. Thus the magnetic form factor of ^{3}He provides the best opportunity known at present to investigate quantitatively the non-nucleonic degrees of freedom of a complex nuclear system. With this objective in mind, the present experiment was undertaken to measure the magnetic cross section with a precision approaching 1% over the range $0.7 < q^2 < 11$ fm^{-2}.

EXPERIMENTAL PROCEDURE

An overview of the experimental arrangement in the electron scattering hall at Bates is shown in Fig. 2. For the magnetic form factor measurements, the spectrometer was set to a scattering angle of 160°. At this angle, the charge contribution to the cross section varies from about 50% at $q^2=1$ fm^{-2} to about 3% at $q^2=10$ fm^{-2}. Thus, at higher values of q^2, only a modest knowledge of the charge form factor is needed to extract the magnetic form factor accurately. To increase the precision at low q^2, the charge form factor was remeasured for q^2 less than 1 fm^{-2}.

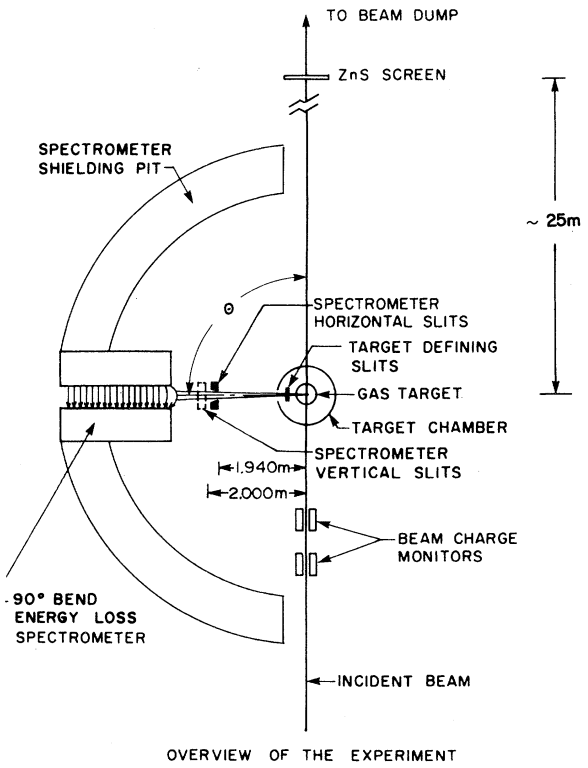

FIG. 2. Overview of the target chamber and spectrometer.

The availability of beam currents up to 50 μamp favors the use of cooled high pressure gas targets, since the density in liquid targets becomes uncertain for currents above 1 μamp due to the formation of bubbles.[3] As will be shown below, corrections to the density in gas targets are small and proportional to the average beam current. In addition, gas targets can be designed so that background due to scattering from the target windows is practically eliminated.

Cross sections were obtained absolutely, in terms of beam charge, target thickness, solid angle, and detector efficiency. Errors in these parameters were limited to 0.5%, as were contributions from the uncertainties in the scattering angle and the beam energy. Thus apart from statistical errors, the measured cross sections have uncertainties of the order of 1%. The methods used to limit the errors are described in detail elsewhere,[6] and will be outlined here. The data were taken in four sets:

a. 160° preliminary. The data from this run have relatively large uncertainties, of the order of 4%, and thus do not satisfy the criteria set forth above. Nonetheless, they have been included in the analysis since they contain the points at highest momentum transfer, where the statistical error is dominant in any case. During this run, target density, beam charge, and detector efficiency were uncertain at the 1% level; scattering angle was not controlled to better than 2 mrad, and the target arrangement allowed some background from window scattering into the spectra. The target gas was pure ^{3}He.

b. 160° checkout. This run was used to study the effect of beam heating on the target density and to measure cross sections of ^{4}He and ^{1}H that could be compared with existing data. The target was a 95/5 molar mixture of ^{4}He and ^{1}H.

c. 160° final. These data were used to verify the normalization of the data from the preliminary run to obtain points at low momentum transfer. As a check on gross errors, hydrogen cross sections were measured at each energy. The target was a 95/5 molar mixture of ^{3}He and ^{1}H.

d. 60° charge. This run was used to measure the charge form factor of ^{3}He for q^2 less than 1 fm^{-2}, and to verify that systematic errors in the cross sec-

tions were within estimates, as evidenced by the value of the form factor for $q^2=0$.

EQUIPMENT

The beam provided by the linac has a total energy spread of 0.3%, but the dispersion matching of the beam and the spectrometer[7] allows resolution of the scattered electron energy loss at the 0.01% level. This resolution is much finer than needed in our case, because the first inelastic channel is the onset of two-body breakup in ^{3}He at 5.5 MeV.

The spectrometer focal plane was instrumented with a multiwire drift chamber backed up by two Cerenkov counters in coincidence.[6,7] In view of the relatively coarse resolution needed, the chamber was used as a multiwire proportional chamber with a resolution equal to the wire spacing, equivalent to 0.07%. The efficiency of the wire chamber was 100%, whereas the efficiency of the Čerenkov counters was between 87% and 97%, depending on the energy. Corrections for dead time effects never exceeded 5%. Overall uncertainty in the efficiency was typically 0.2%.

The angle of the spectrometer relative to the 0° line was established within 0.5 mrad by means of a theodolite mounted on the spectrometer. The beam was aligned within 1 mrad relative to the 0° line by centering it on a removable screen in the target chamber and on a screen mounted in the beam dump, about 24 m downstream from the target chamber. Possible errors in the cross section due to uncertainties in the scattering angle were typically 0.3%.

The beam charge was measured with two torodial monitors placed upstream from the target chamber. The absolute accuracy of the charge measurement was 0.1%.[8]

The incident energy was calculated from the scattered electron energy, which was obtained in turn from the spectrometer magnetic field. Uncertainties in target half-thickness, scattering angle, beam position on target, spectrometer dispersion, and position of the peak on the focal plane contribute small errors, of the order of 0.01%. The principal error is in the bending constant of the spectrometer, which is known to 0.1%. The beam was sufficiently well distributed over the 0.3% acceptance bite that the average and nominal values of the incident energy differed by less than 0.03%. Overall uncertainty in the incident energy was 0.13%, resulting in cross section errors of no more than 0.4%.

Cross sectional views of the targets are shown in Fig. 3. The target of Fig. 3(a) was used at 60° and in the preliminary run at 160°. It consisted of a cylinder fabricated from 6061-T6 aluminum that was machined to form a 0.4-mm wrap-around window, 3.8 cm high and 10 cm in diameter. The machined cylinder was arc welded to a liquid nitrogen reservoir on top and to a cap on the bottom. It has been operated at pressures up to 10 atm and tested at 15 atm.

The target shown in Fig. 3(b) was used at 160° in the checkout and final runs. It was designed to eliminate background due to window scattering and to obtain a higher target density. The windows were hydroformed from 1100-H18 aluminum of 0.4 mm thickness and electron beam welded to the body. The body was surrounded by a liquid nitrogen jacket. It has been tested to 20 atm and operated at 15 atm.

A schematic drawing of the gas handling system is presented in Fig. 4. It consists of an 800 cm^2 diaphragm pump and two pressure gauges with an absolute accuracy of 0.1%. The pump and the meters were connected to the system by means of three-way ball values that allowed them to be isolated or to point to either the reservoir or the target.

At the beginning of a run the reservoir was filled with target gas and the rest of the system evacuated. After filling, the target density was calculated from the reservoir pressure difference, the reservoir temperature, and the ratio of reservoir to target volume, which was measured separately. Small corrections were made for reservoir temperature variations, dead spaces in the transfer apparatus, the second virial coefficient of the target gas, and the contraction of the target at liquid nitrogen temperature. Overall uncertainty in the determination of the target density was 0.2%.

At the end of a run the total amount of gas in the system was determined after the target had warmed up to room temperature. By this means it has been verified that the loss of target gas in the course of a run was under 0.1%.

The arrangement of target and slits used during the runs with the 160° target is shown in Fig. 5. The volume viewed by the spectrometer was limited in the horizontal direction by tungsten defining slits located 25.4 cm from the target center. The slit aperture was 1.27 cm with a taper of 1.3°, somewhat larger than the acceptance of the spectrometer. There were no vertical slits at the target. Antiscatter slits placed close to the target shielded the defining slits from direct view of the beam entrance

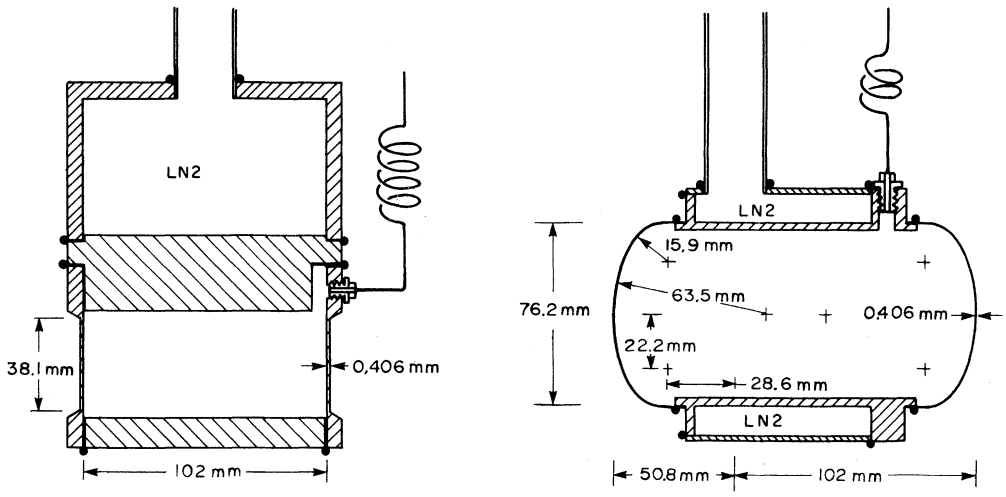

FIG. 3. Cross sections of the high pressure, cooled gas targets.

and exit points on the windows. The antiscatter slits were outside the view of the spectrometer. In order to make the antiscatter slits effective for the exit window, the target was made asymmetrical, with the exit window further from the active region. The effectiveness of the arrangement is shown by the lack of background above the elastic peak in the spectra taken with this target, examples of which are shown in Figs. 6(a) and (c).

Similar slit arrangements were used with the wrap-around target. In the preliminary run at 160°, a slightly different slit geometry and the closeness

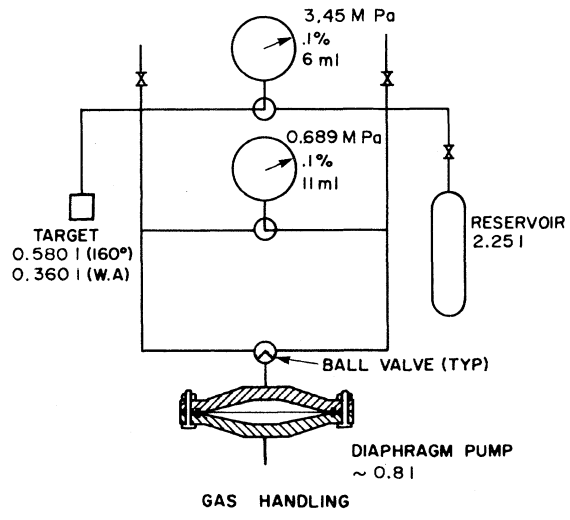

FIG. 4. Schematic representation of the gas transfer system.

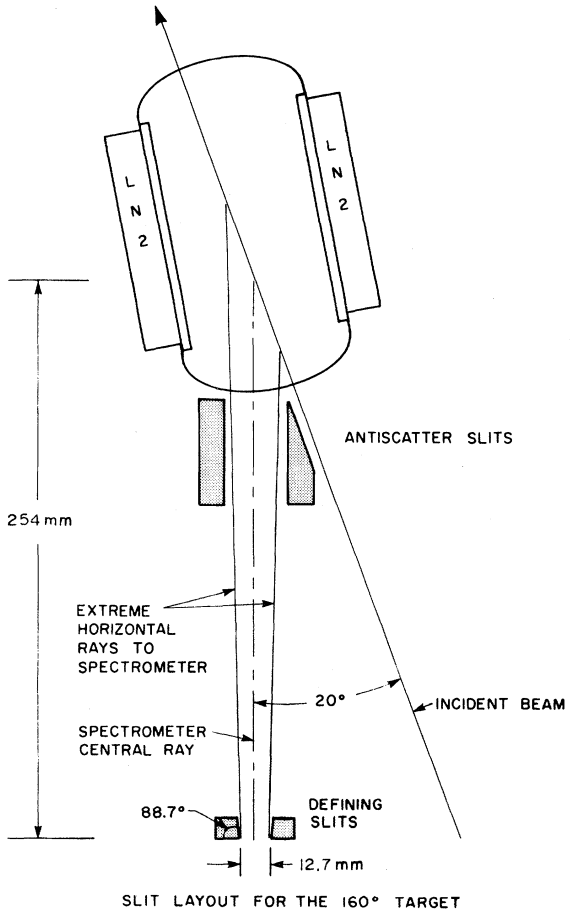

FIG. 5. Geometry of the 160° target and the defining and the antiscattering slits. The slits are constructed from Heavymet.

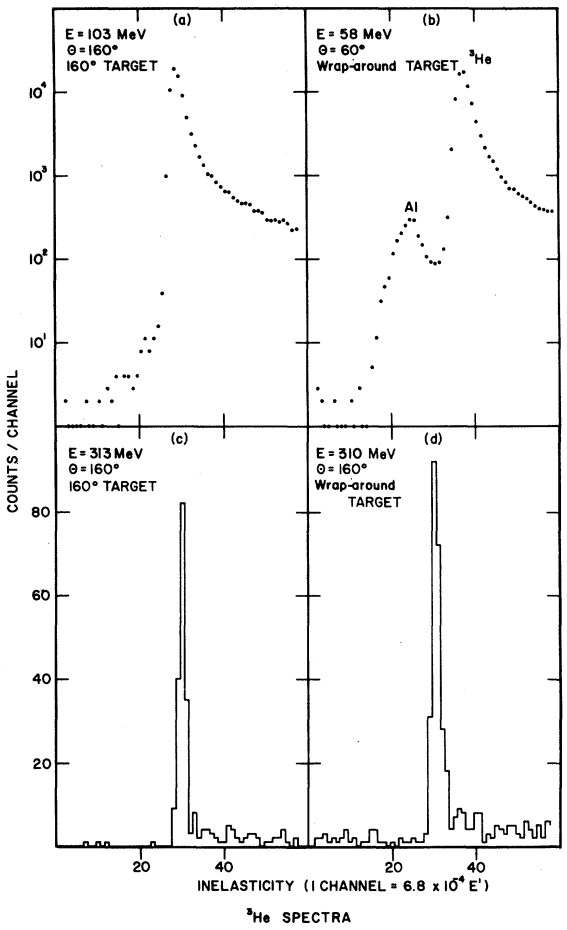

FIG. 6. Measured energy spectra of electrons scattered from ^{3}He at incident electron energies and scattering angles as indicated.

of the exit window allowed some background into the spectra, resulting in corrections to the peak areas that ranged from 1% at 185 MeV to 20% at 380 MeV. A spectrum obtained at 310 MeV is shown in Fig. 6(d). In the run at 60°, some background was produced by double scattering at approximately 30°. The worst case, taken at 58 MeV and shown in Fig. 6(b), required a 1% correction to the peak area.

Corrections for the finite size of apertures were generally small, except in the case of charge scattering at 160°. In this case, the large vertical aperture of the spectrometer, ± 65 mrad, results in an effective scattering angle significantly more forward than the nominal value, and in a corresponding increase in the yield of about 1%. Small corrections, of the order of 0.3%, were also made for multiple scattering in the target gas and in the windows.

The possibility of yield increase from slit edge scattering was investigated by looking for changes in the radiation tail as a function of aperture setting. In agreement with calculations, it was concluded that slit edge scattering has at most an effect of a few percent on the radiation tail for the apertures used, implying a negligible change in the yield.

Beam heating of the target gas reduces the density in the beam path below the no-beam value. This variation was studied for the 160° target at 103 MeV during the checkout run, and for the wrap-around target at 201 MeV during the 60° run. Beam parameters (peak current, pulse width, spot size, and repetition rate) were varied over 10:1 ranges, and it was found that the density correlated with the average current, as indicated in Fig. 7. Straight line fits indicate that, for every 10 μamp of average beam current, the density decreased 1.0 ± 0.14% in the 160° case and 1.1 ± 0.3% in the 60° case. The 60° data, with the exception of the point at 201 MeV where the variation was studied, were taken at currents of about 30 μamp. Thus, the uncertainty in the density due to beam heating was typically 0.4.%

The beam heating effect was also studied for the hydrogen component in the 160° case. In this case, with substantially poorer statistics, the decrease was 0.5 ± 0.5% per 10 μamp of beam current.

DATA ANALYSIS

The cross sections and total form factors presented in Table I were calculated according to the following:

$$\sigma=\frac{N_p(\Delta E)}{\Omega N_e N_t e^{-\delta(\Delta E)}}\ , \tag{1}$$

$$f^2(q^2)=\sigma/\sigma_{\text{Mott}}\ , \tag{2}$$

where $N_p(\Delta E)$ is the corrected number of counts in the elastic peak up to inelasticity ΔE, Ω is the solid angle, N_e is the total number of incident electrons, N_t is the target thickness in nuclei per unit area, $e^{-\delta(\Delta E)}$ is the radiative correction for inelasticity ΔE, σ_{Mott} is the Mott cross section given by

$$\sigma_{\text{Mott}}=\frac{Z^2\alpha^2}{4E^2}\left[\frac{E'}{E}\right]\frac{\cos^2\theta/2}{\sin^4\theta/2}\ , \tag{3}$$

and q^2 is the four-momentum transfer squared, given by

$$q=4EE'\sin^2\theta/2\ . \tag{4}$$

E and E' are the incident and scattered electron en-

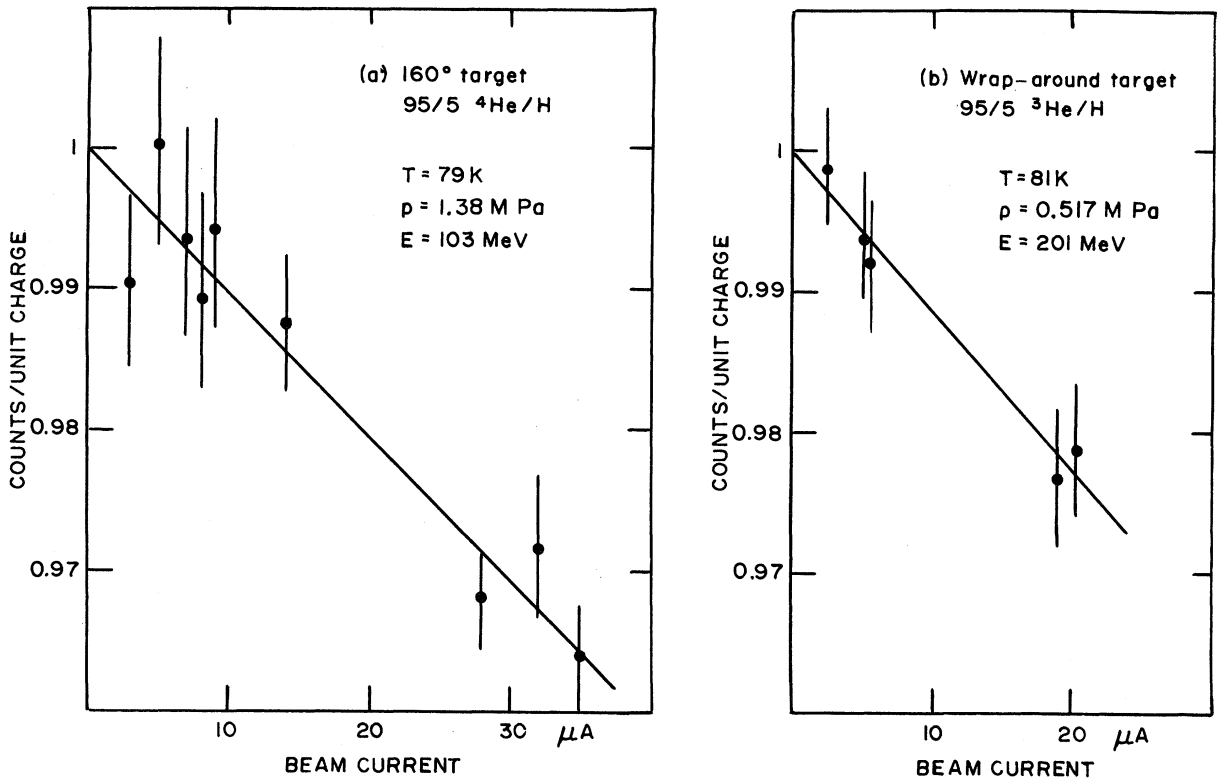

FIG. 7. Relative yield of the ^{3}He elastic peak as a function of average beam current.

ergy, θ is the scattering angle, Z is the atomic number, and α is the fine structure constant.

$N_p(\Delta E)$ was obtained from the raw spectrum of scattered electrons by first subtracting background, if any, and then applying corrections for the following effects: (i) a decrease in target density due to beam heating (2%), (ii) focal plane detector efficiency (5%), (iii) finite aperture effects (0.5%), (iv) multiple scattering (0.5%). The numbers in parentheses give typical values of the corrections.

The radiative corrections were calculated according to the analysis of Bergstrom,[9] modified to take into account the effects of nuclear radiation and recoil and the improved bremsstrahlung calculation discussed by Mo and Tsai.[10] Since the corrections obtained in this manner differed little from those obtained using simpler expressions discussed by Uberall,[11] they have been given in Table II as a product of the simpler expressions and a slowly varying function of the scattered energy.

Where appropriate, we have separated those errors which are common to all measurements of a run and thus contribute to an overall normalization error, from those which vary randomly in sign for each measurement. Some corrections contribute to both categories. The quoted random error was pessimistically estimated by taking the linear sum of random instrumental errors and combining it quadratically with the statistical error. The quoted systematic errors were also pessimistically estimated by taking the geometrical mean of the linear and quadratic sums of the systematic instrumental errors.

We have analyzed the data to extract Born charge and magnetic form factors $F_C(q^2)$ and $F_M(q^2)$, which are the charge and magnetic moment distributions in momentum space. For an extended nucleus of spin $\frac{1}{2}$ and vanishingly small charge, these form factors are defined by the Rosenbluth formula:

$$\sigma/\sigma_{\text{Mott}}=F_C^2(q^2)+(1+2\tan^2\theta/2)\frac{\mu^2}{Z^2}\frac{q^2}{4m^2}F_M^2(q^2)\,, \tag{5}$$

where μ is the magnetic moment in nuclear magnetons and m is the proton mass.

For finite Z, the electron wave function is distorted in the region of the nucleus, and our measurements yielded distorted form factors, f_C and f_M, that depend on q^2 and on θ. We have calculated the ratio of F_C^2 to f_C^2 by phase shift analysis in a re-

TABLE I. Cross section.

^{4}He 160° checkout run				
E (MeV)	q^2 (fm^{-2})	σ (nb/sr)	$f_C{}^2$	Total error (%)
103.42	1.011	23.09	0.392	2.0
^{1}H 160° checkout run				
E (MeV)	q^2 (fm^{-2})	σ (nb/sr)	σ/σ_D	Total error (%)
103.42	0.877	64.0	1.015	2.0
^{1}H 160° checkout run				
E (MeV)	q^2 (fm^{-2})	σ (nb/sr)	σ/σ_D	Total error (%)
85.41	0.618	74.2	0.977	5.0
103.39	0.877	64.1	1.016	5.0
149.35	1.70	42.0	0.996	5.0
184.07	2.44	31.0	0.977	5.0
224.87	3.43	23.1	1.009	5.0
266.52	4.56	15.9	0.964	5.0
289.79	5.23	13.9	1.009	5.0
312.43	5.90	10.8	0.938	5.0
348.65	7.03	8.8	1.008	5.0
^{3}He 60° systematic error 1.5%				
E (MeV)	q^2 (fm^{-2})	σ (μb/sr)	f^2	Random error (%)
58.60	0.0873	66.13	0.922	1.5
89.70	0.2034	24.13	0.793	1.2
109.78	0.3036	14.17	0.700	1.0
141.96	0.5048	6.656	0.553	1.0
174.70	0.7601	3.225	0.408	1.0
201.70	1.0086	1.852	0.314	1.0
^{3}He 160° preliminary run				
E (MeV)	q^2 (fm^{-2})	σ (nb/sr)	f^2	Total error (%)
185.23	3.03	2.43	1.42^{-1}	3.5
216.24	4.05	9.06^{-1}	7.33^{-2}	3.5
238.11	4.85	4.50^{-1}	4.47^{-2}	3.5
257.83	5.62	2.18^{-1}	2.57^{-2}	5.0
271.53	6.19	1.41^{-1}	1.86^{-2}	4.5
283.51	6.70	8.64^{-2}	1.25^{-2}	4.5
298.26	7.35	5.51^{-2}	8.88^{-3}	6.0
309.15	7.85	4.02^{-2}	7.01^{-3}	7.0
319.07	8.31	2.56^{-2}	4.79^{-3}	8.0
328.80	8.78	1.43^{-2}	2.84^{-3}	9.5
368.25	10.78	4.00^{-3}	1.02^{-3}	10.5
377.85	11.28	1.91^{-3}	5.20^{-4}	45.0
^{3}He 160° final run systematic error: 1%				
E (MeV)	q^2 (fm^{-2})	σ (nb/sr)	f^2	Random error (%)
85.41	0.6864	5.925^{+1}	6.885^{-1}	1.0
103.39	0.994	3.273^{+1}	5.639^{-1}	1.0
149.35	2.015	7.678	2.842^{-1}	1.0
184.07	2.995	2.540	1.459^{-1}	1.0
224.87	4.361	6.868^{-1}	6.036^{-1}	1.5
266.52	5.977	1.654^{-1}	2.092^{-2}	2.0
289.79	6.972	7.407^{-2}	1.123^{-2}	3.0
312.43	8.000	3.110^{-2}	5.550^{-3}	5.0
348.65	9.760	8.230^{-3}	1.870^{-3}	12.0

TABLE II. The radiative corrections are given by

$$e^{-\delta(\Delta E)}=(a-bE')(1-1/\omega)(1-\delta_2)(\Delta E/E')(\delta_1+\lambda/\ln 2)\ ,$$

where

$$\delta_1=(2\alpha/\pi)[\ln(q^2/m^2)-1]\ ,$$

$$\delta_2=-(2\alpha/\pi)\{\tfrac{13}{12}[\ln(q^2/m^2)-1]-\tfrac{17}{36}-\tfrac{1}{2}[\pi^2/6-L_2(\cos^2\theta/2)]\}\ ,$$

$$\omega=(\Delta E/\xi)\{1-[\ln(\Delta E/\xi)(1+\Delta E/\xi)]\}\ .$$

L_2 is the Spence function, λ is the thickness of the target in radiation lengths, and ξ is the Landau parameter. $\Delta E/E'$ is always 0.01. Values for λ, ξ, a, b, and other relevant parameters are given below.

Run	60°	160° (preliminary)	160° (checkout)	160° (final)
Target gas	^{3}He/^{1}H	^{3}He	^{4}He/^{1}H	^{3}He/^{1}H
Mole fraction	95/5	100%	95/5	95/5
Density (mol/l)	0.737	1.45	2.09	2.07
λ	0.0095	0.0098	0.0101	0.0101
ξ (keV)	18.5	20.7	22.6	22.6
a	1.003	1.0044	1.0044	1.0044
b	0	4.16×10^{-5}	4.16×10^{-5}	4.16×10^{-5}

cursive manner by using our parametrization of the distorted form factor as the trial distribution of charge and correcting this assumed distribution to yield a new parametrization, etc. The electron wave functions obtained in this calculation have been used to calculate the ratio of $F_M{}^2$ to $f_M{}^2$ in distorted wave Born approximation (DWBA),[11] also in a recursive manner.

The charge form factor was obtained from the total form factor at 60° by assuming that $f_M=f_C$. Negligible error was introduced by this assumption because, for q^2 below 1 fm^{-2}, the magnetic contribution to the cross section is at most 2% at 60°, and the charge and magnetic form factors differ by only 1% or 2%. The values of the Born form factor, presented in Fig. 8 and in Table III, are given by

$$F_C{}^2(q^2)=f^2(q^2)\epsilon_M\epsilon_D\epsilon_N\ , \tag{6}$$

where ϵ_M is the correction for magnetic scattering,

$$\epsilon_M{}^2=\left[1+\frac{\mu^2}{Z^2}\frac{q^2}{4m^2}(1+2\tan^2\theta/2)\right]^{-1}\ . \tag{7}$$

ϵ_D is the distortion correction, and ϵ_N is a normalization factor of 0.995 that minimizes the error of the fit discussed below.

The data for low q compare favorably with the results obtained by Szalata *et al.*[12] at the National

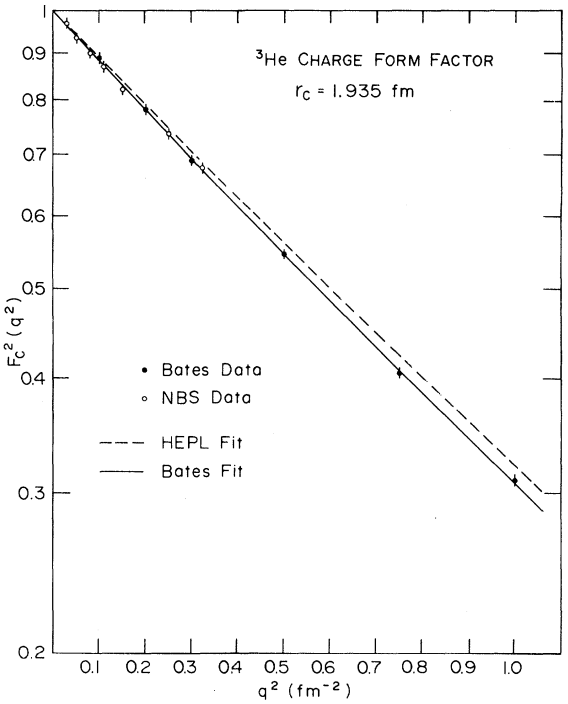

FIG. 8. Experimental values from this work and NBS (Ref. 12) for the charge form factor of ^{3}He vs q^2. The dashed line is the empirical fit to the data of McCarthy *et al.* (Ref. 3) from measurements at higher values of q^2.

TABLE III. Charge form factor. f: total form factor at 60°, ϵ_M: magnetic scattering correction, ϵ_D: Coulomb distortion correction, ϵ_N: normalization correction, F_C: Born form factor, and $F_C{}^2=f^2\epsilon_M\epsilon_D\epsilon_N$.

q^2 (fm^{-2})	f^2	ϵ_M	ϵ_D	ϵ_N	$F_C{}^2$	Random error (%)
0.10	0.908	0.998	0.998	0.995	0.891	1.5
0.20	0.796	0.996	0.991	0.995	0.782	1.2
0.30	0.703	0.994	0.993	0.995	0.690	1.0
0.50	0.556	0.990	0.997	0.995	0.546	1.0
0.75	0.413	0.984	1.002	0.995	0.405	1.0
1.00	0.317	0.979	1.005	0.995	0.310	1.0

Bureau of Standards (NBS). For clarity of presentation, the NBS data shown in Fig. 8 have been smoothed by averaging nearby points. For q^2 below 1 fm^2, a form factor of the type

$$F_C(q^2)=(1+a^4q^4)\exp[-(r_C{}^2q^2/6)] \tag{8}$$

is sufficient to account for the data. A joint fit of the NBS and Bates data with this form factor, with allowance for a separate normalization for each data set, yielded $a^4=0.038\pm0.005$ fm^4 and an rms radius r_C of 1.935 ± 0.03 fm. To obtain the best fit, the NBS cross sections were raised by 0.2%, whereas the Bates cross sections were lowered by 0.5%, indicating that the estimate of systematic error, 1.5%, is generous.

The charge form factor measurements of McCarthy *et al.*[3] at High Energy Physics Laboratory (HEPL) are summarized by their best fit form factor,

$$F_C(q^2)=\exp(-a^2q^2)-b^2q^2\exp(-c^2q^2) -d\exp\{-[(q-q_0)/p_0]^2\}\,, \tag{9}$$

with $a^2=0.4556$ fm^2, $b^2=0.1340$ fm^2, $c^2=0.6989$ fm^2, $d=0.00678$, $q_0=3.98$ fm^{-1}, and $p_0=0.9$ fm^{-1}. This form factor is shown by the dashed line in Fig. 8, where it can be seen that it disagrees appreciably with the Bates data.

To obtain a form factor usable over the range 0–10 fm^{-2} that would take into account the new Bates data and yet respect the main features of the HEPL measurements, the Bates data were fit with a form factor parametrized like the HEPL form factor, allowing for variation of the parameters a, b, and c that determine the low q behavior, but keeping the HEPL values for the remaining parameters that define high q behavior. The parameters a, b, and c were varied subject to the constraints that the rms radius be 1.935 fm, as required by the Bates and NBS data, and that the zero in the form factor occur at 11.6 fm, as required by the HEPL data. The resulting values of the parameters were $a^2=0.461$ fm^2, $b^2=0.163$ fm^2, and $c^2=0.765$ fm^2.

The HEPL-like form factor obtained above differs the most from the HEPL best fit at $q^2=2$ fm^{-2}, by about 2%, and thereafter rejoins it, so that they are practically identical for q^2 above 6 fm^{-2}. Since it is reasonable to assume that the discrepancy between the HEPL and the Bates data does not vanish beyond the range tested here, it was assumed that the percent error of the charge contribution to the cross section at 160° was numerically equal to q^2 for q^2 measured in fm^{-2}.

The distorted magnetic form factor is given by

$$f_m{}^2(q^2)=\frac{f^2(q^2)-f_C{}^2(q_2)}{\frac{\mu^2}{Z^2}\frac{q^2}{4m^2}(1+2\tan^2\theta/2)}\,, \tag{10}$$

where f_C is calculated using a phase shift code. The Born magnetic form factor is given by

$$F_M{}^2(q^2)=\epsilon_D f_M{}^2(q^2)\,, \tag{11}$$

where ϵ_D is the ratio of $F_M{}^2$ to $f_M{}^2$ calculated with a DWBA code. Born magnetic form factor values are presented in Table IV and in Fig. 9. The error bars take into account only the random error in the cross sections.

The normalization error in the cross sections from the final 160° run was estimated to be less than 1%. This estimate is supported by the 60° data which, with an estimated 1.5% normalization error, have been shown above to be in error by no more than 0.5%. The cross sections of ^{4}He and ^{1}H measured during the checkout run also indicated that a 1% estimate of systematic error is sensible, although the proof was not conclusive because the data used for comparison are uncertain at 2% level.

The current experimental situation for ^{4}He has been summarized by McCarthy *et al.*[3] who included in their analysis, in addition to their own data, the results of previous measurements at HEPL by Frosch *et al.*[13] and the low q data from

TABLE IV. Magnetic form factor. $f_M{}^2=(f^2-f_C{}^2)/(0.8174q^2)$, $F_M{}^2=\epsilon_D f_M{}^2$, and ϵ_D is the distortion correction.

(fm^{-2})	f^2	$f_C{}^2$	$f_M{}^2$	ϵ_D	$F_M{}^2$	Random error (%)
0.686	6.89^{-1}	4.40^{-1}	4.43^{-1}	0.980	4.34^{-1}	3.0
0.994	5.64^{-1}	3.08^{-1}	3.15^{-1}	0.990	3.12^{-1}	2.5
2.015	2.84^{-1}	1.03^{-1}	1.10^{-1}	1.012	1.12^{-1}	2.0
2.995	1.46^{-1}	3.89^{-2}	4.37^{-2}	1.029	4.50^{-2}	1.5
4.361	6.04^{-2}	1.10^{-2}	1.39^{-2}	1.047	1.45^{-1}	2.0
5.977	2.10^{-2}	2.55^{-3}	3.76^{-3}	1.068	4.02^{-3}	2.5
6.972	1.12^{-2}	1.02^{-3}	1.79^{-3}	1.080	1.93^{-3}	3.0
8.000	5.55^{-3}	3.72^{-4}	7.92^{-4}	1.093	8.66^{-4}	5.0
9.760	1.87^{-3}	4.20^{-5}	2.29^{-4}	1.114	2.55^{-4}	12.0
3.03	1.42^{-1}	3.75^{-2}	4.20^{-2}	1.028	4.32^{-2}	5.0
4.05	7.33^{-2}	1.45^{-2}	1.78^{-2}	1.043	1.85^{-2}	4.0
4.85	4.47^{-2}	7.04^{-3}	9.50^{-3}	1.054	1.00^{-2}	4.0
5.62	2.57^{-2}	3.52^{-3}	4.82^{-3}	1.063	5.12^{-3}	6.0
6.19	1.86^{-2}	2.10^{-3}	3.26^{-3}	1.070	3.49^{-3}	5.0
6.70	1.25^{-2}	1.31^{-3}	2.04^{-3}	1.076	2.20^{-3}	5.0
7.35	8.88^{-3}	7.10^{-4}	1.36^{-3}	1.084	1.47^{-3}	6.5
7.85	6.98^{-3}	4.35^{-4}	1.02^{-3}	1.090	1.11^{-3}	7.5
8.31	4.79^{-3}	2.67^{-4}	6.65^{-4}	1.096	7.29^{-4}	8.5
8.78	2.84^{-3}	1.58^{-4}	3.73^{-4}	1.102	4.11^{-4}	10.0
10.78	1.02^{-3}	1.00^{-5}	1.16^{-4}	1.126	1.31^{-4}	10.5
11.28	5.20^{-4}	1.00^{-5}	5.60^{-5}	1.132	6.30^{-5}	45.0

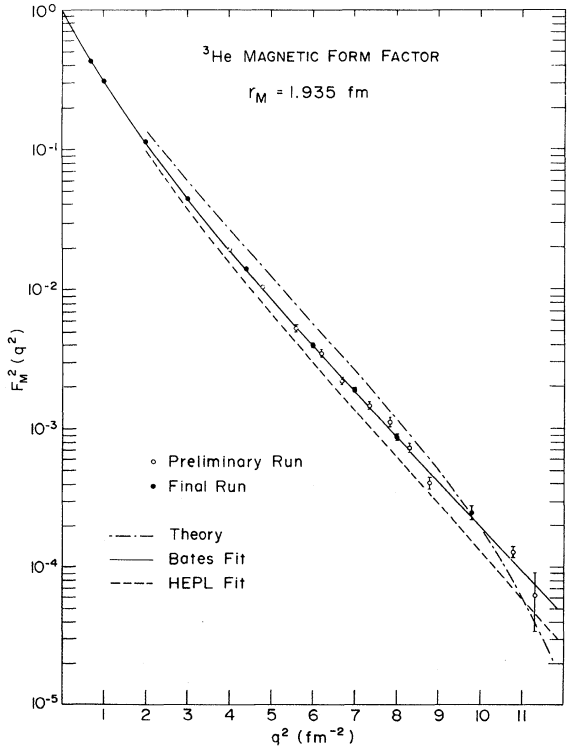

FIG. 9. Experimental values of the magnetic form factor of ^{3}He from this work. The HEPL empirical fit (Ref. 3) and our empirical fit are shown for comparison.

Darmstadt.[14] For low q, the form factor can be calculated from a Gaussian charge distribution with an rms radius of 1.762 ± 0.025 fm. At 103.42 MeV and 160° this distribution predicts a cross section of 22.95 ± 0.65 nb, which agrees within 0.5% with our measured value, 23.09 ± 0.46 nb.

The available hydrogen data have been reanalyzed recently by Höhler *et al.*[15] At 160°, where the cross section is strongly dominated by the magnetic contribution, use of the dipole fit form factor

$$F_D(q^2)=[1+q^2(f_m{}^{-2})/18.23]^{-2} \tag{12}$$

for both the charge and magnetic form factors gives a fair representation of the data. Since previous analyses[16] of hydrogen data indicated form factors that decrease faster than the dipole parametrization and no analysis takes into account distortion corrections that modify the form factors at the percent level, it was considered here that calculated hydrogen cross sections have an uncertainty of 2%.

The hydrogen cross section measured in the checkout run at 103.42 MeV is 64.0 ± 0.12 nb, 1.5% higher than the value predicted by the dipole fit. The hydrogen cross sections measured during the final 160° run were intended to check for gross deficiencies, and not for accurate normalization, since

the hydrogen peak lies on considerable background from the breakup bump in ^{3}He and the subtraction errors are of the order of 3%. In addition, the fraction of hydrogen in the target gas is known only to 1% in this case, and the density corrections due to beam heating have an uncertainty of 2%. The measured cross sections, presented as ratios to the dipole fit predictions in Fig. 10, do not indicate unexpected discrepancies, but they should not be considered as a measurement of hydrogen form factors.

A least squares fit to the magnetic form factor data with a function of the type

$$F_M(q^2)=a^2e^{-b^2q^2}+(1-a^2)e^{-c^2q^2} \quad (13)$$

yielded parameters $a^2=0.5710$, $b^2=0.3705$ fm^2, and $c^2=0.9615$ fm^2. The χ^2N of the fit is 0.88 per degree of freedom, and the rms radius of the corresponding magnetization distribution is 1.935 ± 0.01 fm. If the data from the final run were fit separately, the resulting fit function would differ negligibly from the joint fit function for $q^2<8$ fm^{-2}. If the data from the final run were displaced by assuming simultaneous errors of 1% in the cross sections and of q (fm^{-2}) % in the charge contribution, the shift in the fit function would be at most 1.5% and the change in the radius 0.04 fm. With all errors taken into consideration, the parametrization of the Born magnetic form factor given above was estimated to be accurate to 1.5% if q^2 is below 10 fm^{-2}. The rms radius of the magnetic distribution was estimated to be $r_M=1.935\pm0.04$ fm.

CONCLUSION

The charge form factor of ^{3}He has been measured with an accuracy of 0.5% for q^2 below 1 fm^{-2}. In this region it disagrees appreciably with the data of Ref. 3, but it agrees with the data from NBS. The measured rms radius, 1.935 ± 0.03 fm, is compatible with the previously measured value 1.88 ± 0.05 fm.[3,12]

The magnetic form factor of ^{3}He has been measured with an accuracy of 1.5% for q^2 below 10 fm^{-2}. Disagreement with the data of Ref. 3 is quite large, about 15% at $q^2=5$ fm^{-2}. The measured magnetic radius, 1.935 ± 0.04 fm, is in agreement with previous results.[3]

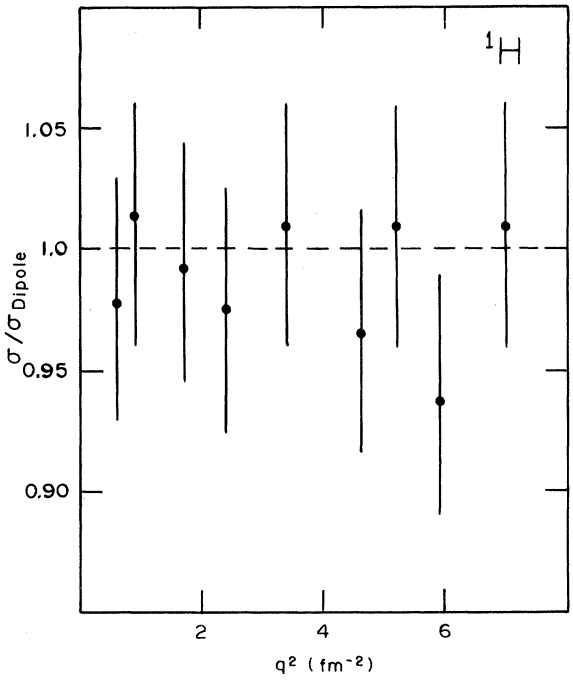

FIG. 10. Ratio of measured hydrogen cross sections relative to the predicted cross section vs q^2. The cross sections are predicted by the dipole fit to the hydrogen electron scattering data.

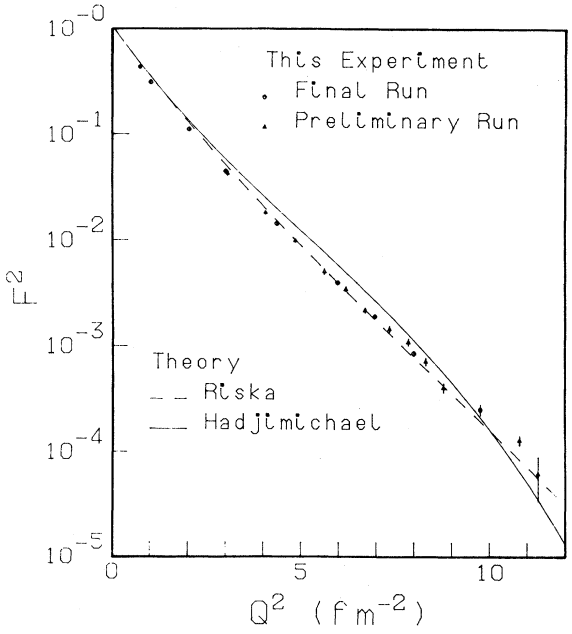

FIG. 11. Measured magnetic form factors of ^{3}He vs q^2 from this work compared with the theory of Riska (Ref. 5) and Hadjimichael (Ref. 17). The latter theory includes the effect of three-body forces but does not include ρ-seagull terms.

Our experimental results for the magnetic form factor are compared with the model calculations of Hadjimichael[17] and Riska[5] in Fig. 11. The agreement of these theories with our results is generally within 5%.

Recently Saclay has made measurements of the ^{3}He magnetic form factor in the range from 8 to 32 fm^{-2}. Their results[18] are in agreement with ours in the region in which there is overlap.

This work was supported in part by the National Science Foundation Grant No. PHY-7715270 and by Department of Energy Contract No. EY-76-C-02-3069.

---

*Current address: National Instituut voor Kernfysica em Hoge-Energiefysica (NIKHEF), Sectie K, Amsterdam, The Netherlands.

†Current address: Fermi National Accelerator Laboratory, Batavia, IL 60510.

[1]M. I. Haftel and W. M. Kloet, Phys. Rev. C 15, 404 (1977).

[2]H. Collard *et al.* Phys. Rev. 138, B57 (1965).

[3]J. S. McCarthy, I. Sick, and R. R. Whitney, Phys. Rev. C 15, 1396 (1977).

[4]A. Barroso and E. Hadjimichael, Nucl. Phys. A238, 422 (1975).

[5]D. O. Riska, Nucl. Phys. A350, 227 (1980).

[6]P. C. Dunn. Ph.D. thesis, Harvard University, 1980 (unpublished).

[7]W. Bertozzi *et al.*, Nucl. Instrum. Methods 141, 458 (1977).

[8]P. C. Dunn, Nucl. Instrum. Methods 165, 163 (1979).

[9]J. Bergstrom, in MIT 1967 Summer Study, USAEC Publ. ITD-24667 (unpublished).

[10]L. M. Mo and Y. S. Tsai, Rev. Mod. Phys. 41, 205 (1969).

[11]H. Uberall, *Electron Scattering from Complex Nuclei* (Academic, New York, 1971).

[12]Z. M. Szalata *et al.*, Phys. Rev. C 15, 1200 (1977).

[13]R. F. Frosch, J. S. McCarthy, R. E. Rand, and M. R. Yearian, Phys. Rev. 160, 874 (1967).

[14]U. Erich, H. Frank, D. Haas, and H. Prang, Z. Phys. 209, 208 (1968).

[15]G. Höhler *et al.*, Nucl. Phys. B114, 505 (1976).

[16]F. Borkowski, P. Peuser, G. G. Simon, V. H. Walther, and R. D. Wendling, Nucl. Phys. A222, 269 (1974); B93, 461 (1975).

[17]E. Hadjimichael, J. Bornais, and B. Gouland, Phys. Rev. Lett. 48, 583 (1982).

[18]J. M. Cavedon, B. Frois, D. Goutte, M. Huet, Ph. Lecomte, J. Martino, X. H. Phan, S. K. Platchkov, S. E. Williamson, W. Boeglin, I. Sick, P. de Witt-Huberts, L. S. Candman, and C. N. Papanicolas, Phys. Rev. Lett. 48, 986 (1982).